

Near-IR demonstration of adaptive nuller based on deformable mirror

Robert D. Peters*, Oliver P. Lay, Muthu Jeganathan, Akiko Hirai
Jet Propulsion Laboratory, California Institute of Technology
4800 Oak Grove Drive, Pasadena CA 91109

ABSTRACT

Deep, stable nulling of starlight requires careful control of the amplitudes and phases of the beams that are being combined. The detection of earth-like planets using the interferometer architectures currently being considered require that the electric field amplitudes are balanced at the level of $\sim 0.1\%$, and the phases are controlled at the level of 1 mrad (corresponding to ~ 1.5 nm for a wavelength of 10 microns). These conditions must be met simultaneously at all wavelengths across the science band, and for both polarization states, imposing unrealistic tolerances on the symmetry between the optical beamtrains. Lay et. al. proposed the concept of a compensator that is inserted into the beamtrain, which can adaptively correct for the mismatches across the spectrum, enabling deep nulls with realistic, imperfect optics. This proposed design uses a deformable mirror (DM) to adjust the amplitude and phase of the electric field that couples into the single-mode spatial filter. The Terrestrial Planet Finder (TPF) has baselined the DM-based compensator for slow correction of spectral asymmetries in amplitude and phase between the beams. Consequently, a testbed is being built to demonstrate accurate phase and amplitude control in the mid-IR by 2006. We have demonstrated amplitude and phase control at a single wavelength in the near-IR. We are preparing to demonstrate control with our deformable mirror actuator in the near-IR, and in parallel are preparing a demonstration in the mid-IR where the compensator will be required to operate.

Keywords: Nulling interferometry, planet detection

1. INTRODUCTION

There is currently a large effort to directly detect Earth-like planets around nearby stars. Direct detection requires a combination of starlight suppression and high angular resolution (< 0.1 arcsec). The technique of nulling interferometry [1] has been proposed at mid-infrared wavelengths for both the European Darwin mission [2] and NASA's Terrestrial Planet Finder (TPF) [3]. The latter is also considering a visible coronagraph architecture.

For the case of the mid-IR interferometer, the light from the star must be suppressed by a factor of 10^5 or more over the bandwidth of interest, currently 7 - 17 μm . All designs under consideration include a single-mode spatial filter (SMSF), through which the combined light is passed before being detected. The wavefront from the star is incident on the collecting apertures of the instrument and delivered by the respective beam trains to a central beam combiner, that couples the light into the SMSF. With just a single mode (actually two – one for each polarization state), the problem is simple to state. The electric field within the SMSF is the vector sum of the electric field contributions from each collecting aperture. The starlight is nulled when the electric fields in the SMSF sum to zero, requiring specific combinations of the electric field amplitude and phase.

Recent analysis [4] shows that the stability of the null that drives the requirements on the accuracy of the amplitude and phase control. The detection of an earth-like planet around a sun-like star at 15 pc requires that the electric field amplitudes are matched to within $\sim 0.1\%$ (intensities equal to within 0.2%), and the phase is controlled to ~ 1 mrad (1.5 nm at a wavelength of 10 μm), simultaneously at all wavelengths and both polarization states. A number of effects can perturb the amplitude coupling into the SMSF, including reflectivity, beam shear, and wavefront aberration: tilt, focus, astigmatism, coma, etc. The phase is obviously impacted by changes in the optical path, but also by birefringence and dispersion introduced by the ~ 30 optical elements present in each beam train.

One approach to architecting the instrument is to attempt to make the beam trains as identical as possible, by applying very tight requirements to the alignment and specification of the optical elements (Fig 1a). Error budgeting shows that

* Robert.D.Peters@jpl.nasa.gov; phone 1 818 393-6263

the tolerances involved are prohibitive. The solution is a technique that we call Adaptive Nulling, in which a compensator is included in each beam train to correct for imbalances in the amplitude and phase, independently at each wavelength and polarization (Fig. 1b)[5,6].

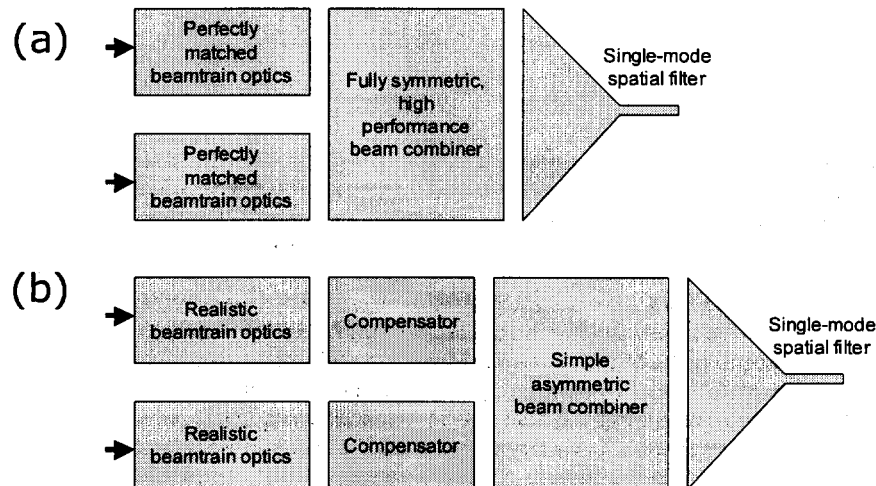


Fig.1. (a) A deep starlight null requires extremely well-matched beamtrain optics and a high performance symmetric beam combiner. (b) Inserting a compensator to correct for amplitude and phase perturbations relaxes the requirements on the beamtrains to more realistic levels and allows a simpler beam combiner design.

In this paper, we present results from a proof-of-concept visible/near-IR DM-based compensator. We are using a LED source with 100nm bandwidth and a commercial spectrometer to demonstrate amplitude and phase control in the near-IR. Equilateral prisms and Wollaston prisms are used to first separate the spectral and polarization components, and then recombine them after adjustment. A 12x12 MEMS deformable mirror (DM) array will be used to adjust the phase (piston) and amplitude (tilt). A simple interferometer (with a delay line) has been built to measure phase and amplitude asymmetries, and demonstrate nulling. We will describe the compensator optical design, phase extraction algorithm, DM characteristics, and control algorithm for adjusting the DM. Null performance improvement with and without correction will be presented by purposely adding phase and amplitude errors in one arm of the interferometer. In section 2, we will present an overview of the Adaptive Nuller concept, then in section 3, we will present what has been done to date on the visible/near-IR proof-of-concept experiment. Finally, in section 4 we shall present the mid-IR work being done in parallel with the proof-of-concept experiment, and a preliminary design of a mid-IR compensator to be built in 2005.

2. CONCEPT OVERVIEW

Table 1 illustrates the requirements we have adopted on compensator performance for integration with Terrestrial Planet Finder. In addition to the science band of 7 – 17 μm , the compensator must pass the metrology wavelength, which is likely to be in the range of 0.5 – 2 μm . At least 6 spectral degrees of freedom are required (λ^0 , λ^{-1} , λ^{-2} dependences for each of amplitude and phase), but more degrees of freedom are desirable given the number of unknown effects.

#	Requirement	
1	Wavelength range of operation	7-17 μm
2	Metrology wavelength	0.5-2 μm
3	# independent spectral degrees of freedom	> 5 (20)
4	# independent polarization states	2
5	Null depth across the band	< 10^{-5}
6	Amplitude correction range	> 5%
7	Amplitude precision / stability (1σ)	< 0.1%
8	Phase correction range	> 2 μm
9	Phase precision / stability (1σ)	< 1 nm
10	Throughput reduction	< 20%
11	Polarization isolation	> 50 dB

Table 2. Performance requirements for adaptive nulling compensator.

The compensator should ideally act independently on the horizontal and vertical polarization states, and support a null depth of 10^{-5} . The null stability requirement leads to the amplitude and phase stability requirements of 0.1% and 1 nm, respectively. A maximum amplitude correction of 5% gives a dynamic range of 50 for amplitude, and the 2 μm phase correction range corresponds to a phase of 0.6 radians at a wavelength of 20 μm . The compensator should have high throughput, and it should not mix the polarization states at more than the 10^{-5} level.

One approach to implementing a compensator is to use a “serial cascade” of correcting elements. Each element has a different spectral response to amplitude and/or phase, with an adjustable gain. An example is depicted schematically in Fig. 2.

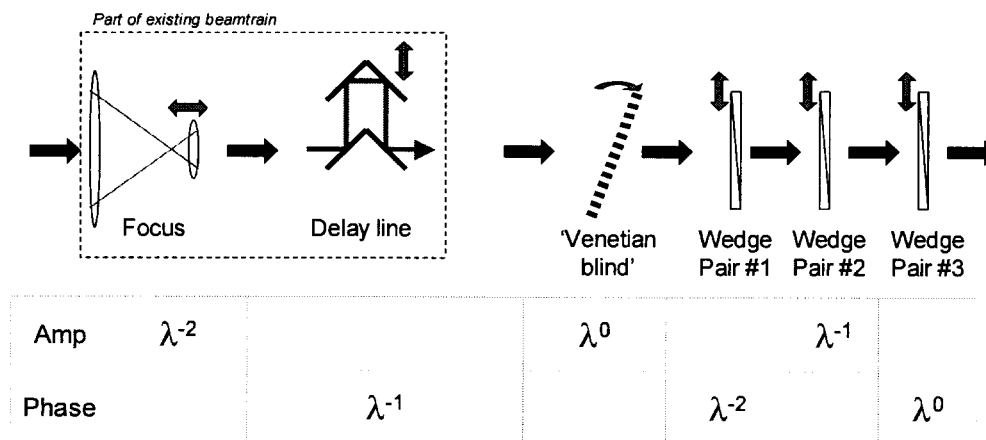


Fig. 2. Example of a serial cascade design for the compensator. The table below indicates the spectral dependence controlled by each element. The wedge pairs provide an adjustable thickness of material through which the beam propagates, with properties chosen to provide the desired spectral dependence.

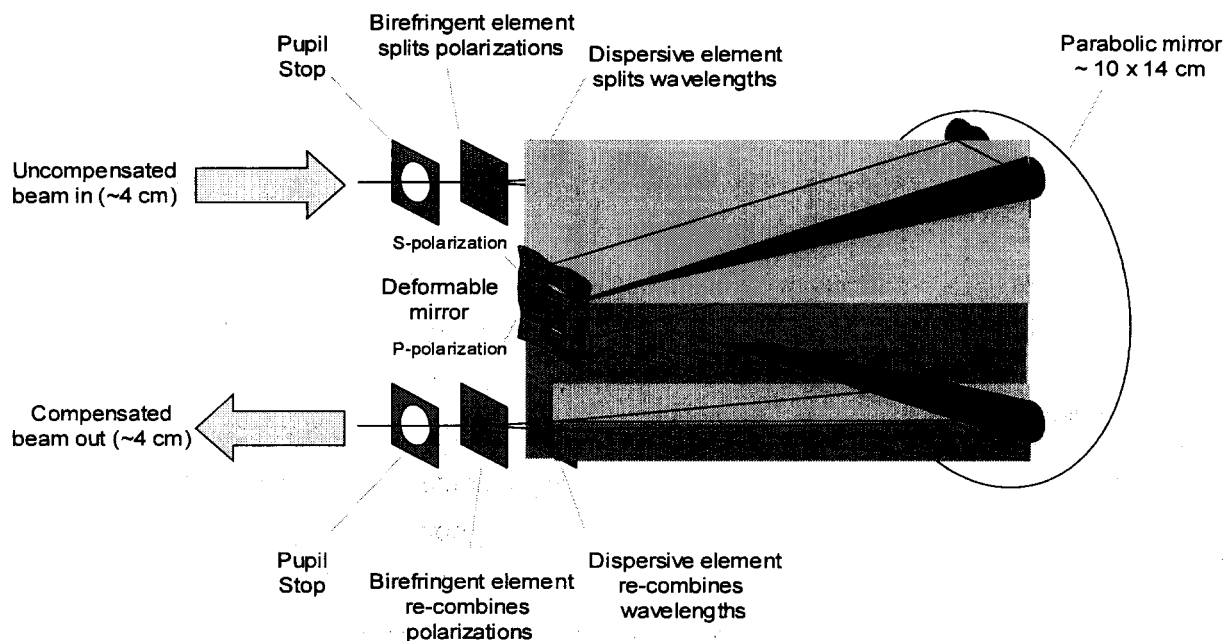


Fig. 3. Parallel, high-order compensator design, using a DM to control amplitude and phase.

The serial cascade approach is best suited to a low-order compensator, i.e. one with relatively few degrees of freedom. As shown in Fig. 2, it does not provide independent control of the different polarization states, although this capability could be added by introducing more elements. The throughput is clearly impacted as more elements are added, since all the photons, irrespective of their wavelength, must pass through all the elements.

An alternative approach is to split the light into the different wavelength and polarization states and operate on them in parallel before recombining them. In principle, it is then possible to implement a high order compensator (many spectral degrees of freedom) without a large impact on throughput. Such a compensator is illustrated in Fig. 3.

The uncorrected beam, with diameter ~ 4 cm, enters at the upper left, passes through a pupil stop, and then through a birefringent element that splits the polarization states by a small angle. The light is then dispersed by a prism and is incident on a parabolic mirror that focuses the collimated beams onto a DM. At this point the input light is spread into two focused lines, one for each polarization state, dispersed by wavelength. After reflection from the DM, the light is re-collimated by the parabolic mirror, de-dispersed and the two polarization states are re-combined before passing through the exit pupil stop.

The DM allows independent control of the amplitude and phase for each polarization and wavelength, as illustrated in Fig. 4. Piston of the DM adjusts the phase of the output beam (Fig. 4a); changing the local slope of the DM at the focal point introduces a shear of the outgoing collimated beam, which is then converted into a reduction of amplitude by the exit pupil stop (Fig. 4b). The piston and local slope are adjusted independently for the different wavelengths and polarization.

This compensator is part of a control system for balancing the amplitudes and phases of the incoming beams. Also needed is a sensor for detecting the imbalances and an algorithm to make the appropriate adjustment at the DM. Since we are correcting for imbalances across the science band, the sensor must operate over the same range of wavelengths. There are at least 3 options:

1. Monitor the null depth directly at the science detector, in each of the spectral channels. The advantages are that no additional sensors are needed, there are no uncommon path effects, and there is no interruption of the science data. One disadvantage is that an iterative adjustment of amplitude and phase is needed to minimize the null

depth. Another is that the null depth for the star is masked by the photons from the exo-zodiacal and local zodiacal dust, and by the thermal emission of the instrument, so that the measurement is not particularly sensitive.

2. Measure the amplitudes and phases of the different beams at regular intervals of time. The science observing must be interrupted to do this. Amplitude is obtained by measuring the photon rate at the science detector for each beam in turn (i.e. block all but one of the beams). Phase is determined by measuring the photon rates obtained for pairs of beams. No additional sensors are needed, there are no uncommon path effects, and the amplitude and phase are being sensed separately. The main disadvantage is that the time available for science observations is reduced.
3. Monitor the amplitudes and phases of the beams by splitting off some of the science light before the beams are combined and using separate detectors. As for the previous option, the amplitudes and phases are measured directly. Disadvantages are that science photons are being diverted to this purpose, there can be substantial uncommon path effects, and additional sensors are required.

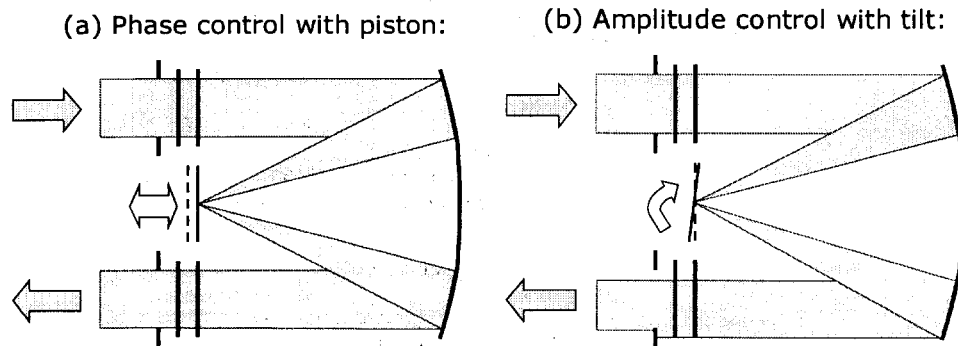


Fig. 4. Phase and amplitude control with a DM. Schematic represents a side view of Fig. 3 with beams shown for a single polarization and wavelength.

Achieving the 0.1% and 1 mrad levels of performance will only be possible at low bandwidth, $f \ll 0.1$ Hz, much slower than the bandwidths for path and pointing control ($f \sim 100$ Hz). Adaptive nulling is a quasi-static correction, which is not a problem if the sources of asymmetry (Table 1) are not changing on short timescales. The correction algorithm will depend on the nature of the sensor, and will need to account for any cross-coupling effects between the amplitude and phase control.

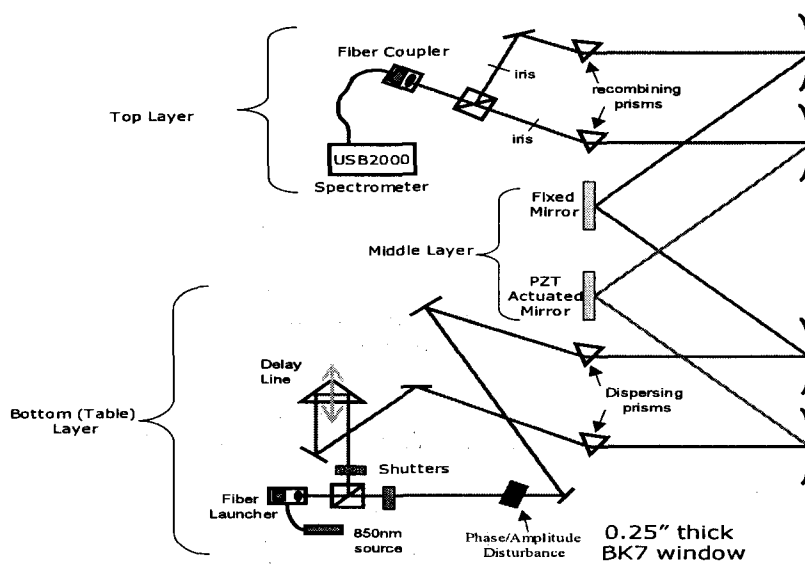


Fig 5: Schematic layout for the visible/near-IR proof-of-concept demonstration. The bottom layer holds the source and delay line, the middle layer holds the actuated mirror and reference fixed mirror, and the top layer is where the beams are combined and coupled into single mode fiber.

3. VISIBLE/NEAR-IR DEMONSTRATION

Due to the long lead-time and cost of items needed for a full demonstration at mid-IR wavelengths, it was decided that a proof-of-concept demonstration at visible/near-IR wavelengths would be done first. Components for the visible/near-IR experiment were readily available and relatively inexpensive. The goal of this demonstration was to design a system similar to that which would be used in the mid-IR, with spot sizes scaled with the wavelength. This demonstration would allow us to begin trying phase and amplitude mismatch extraction algorithms and control while we were working on a mid-IR demonstration in parallel.

Fig. 5 shows the schematic layout for the visible/near-IR demonstration. As indicated in the figure, it is built on three levels. The bottom level holds the source and delay line. The source is a high intensity LED that is coupled into a single mode fiber. The output power is about 0.5 uW with 100nm of usable bandwidth. The delay line is a large retro-reflector with two levels of actuation. The coarse actuation is done by a computer controlled linear stage with 50 mm of travel and 0.1 um resolution. The fine level is done with a PZT actuator, which in the future will be coupled with a simple metrology system to take out air-path variations.

The middle layer holds our actuated mirror and reference mirror for the two arms of our interferometer. The arm with the actuated mirror is the compensator as shown in Fig. 3. The reference arm is the same except it uses a fixed flat mirror instead of an actuated mirror. The actuator we chose was a 3mm square 140 pixel deformable mirror with a custom 12 bit resolution digital driver and ~ 2um stroke from Boston Micromachines. However, due to the long lead-time of the custom electronics, initial testing was done with a PZT actuate 3-degree-of-freedom flat mirror which is what is shown in the figure. Therefore, in these initial tests we could correct for amplitude and phase of a single wavelength.

On the top level, the beams from both arms are combined with a beamsplitter and the nulled output is coupled into a single mode fiber. The signal is then detected with a computer controlled spectrometer based on a linear CCD with 2048 pixels and a resolution of ~0.37nm. We can create a null by combining the adaptive compensator, which is set up as in Fig. 3, and the reference arm, which is set up the same as the adaptive compensator with the only difference being a fixed flat mirror instead of an actuated mirror.

For the proof-of-concept demonstration, we used an equilateral (60 degree) fused silica prism for wavelength separation and a custom quartz Wollaston prism for polarization separation. The Wollaston prism was designed for a polarization (*s* & *p*) separation of 0.1 degree, corresponding to a wedge angle of approximately 5 degrees. Figure 6a below shows the

results from a ZEMAX model of the NIR setup. As can be seen from the spot diagram at the focus of the parabolic mirror, the LED spectrum from 800-900 nm is spread over 2 mm corresponding to 8 pixels on the Boston Micromachines DM. Figure 6b shows the line spread function, that is the intensity distribution for one of the polarizations. For modeling purposes, 5 discrete wavelengths were used, however in the experiment the LED spectrum is continuous. The slightly lower intensity at the longer wavelength is due to the diffraction limited spot size.

To verify the optical design, we placed a standard Si CCD camera at the plane of the DM. The wavelength and polarization dispersion is shown in Figure 7. We see a good agreement with the dispersion compared to Fig 6a. Figure 6b shows the dispersion with the polarizations separated with the Wollaston prism.

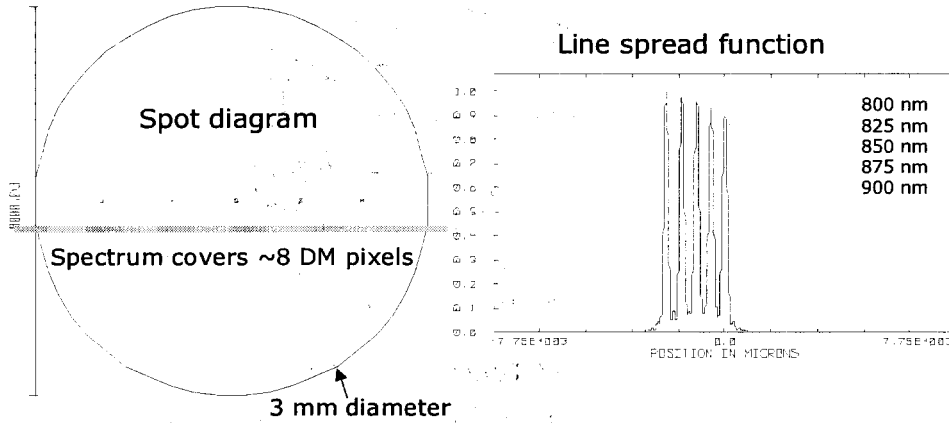


Fig. 6: a) Zemax model of dispersion with the visible/near-IR demonstration along with the size of the pixels on the DM. b) Cross section through the dispersed light. For modeling purposes, 5 discrete wavelengths were used, however the LED used in the experiment produces a continuous spectrum.

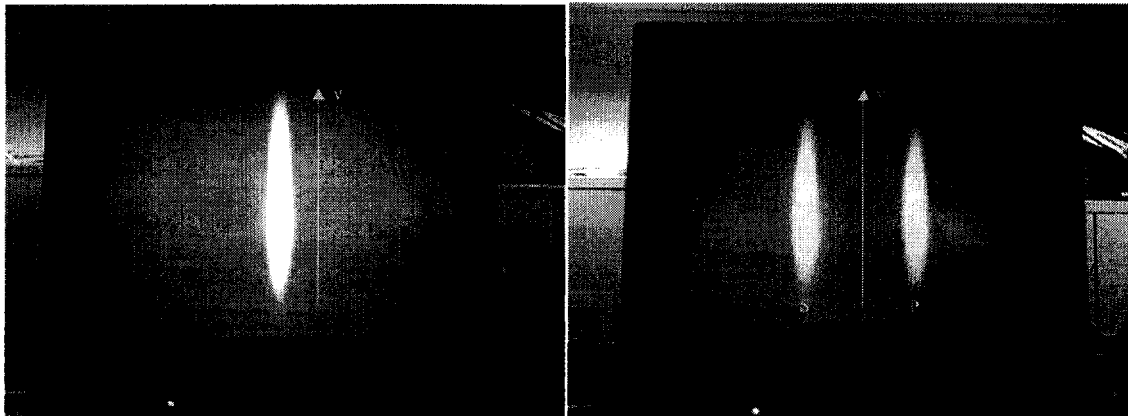


Fig. 7: Bare CCD image of the wavelength dispersion (left) and the wavelength dispersion with the polarization splitting (right).

Measuring amplitude errors is straightforward. One can measure the spectrum of each beam by shuttering the other beam off. We used the difference divided by the sum of the two spectrums as a measure of the intensity imbalance. Once the coupling loss vs. tip/tilt angle is calibrated we can apply the appropriate control signals to match the intensities at a particular wavelength. Fig. 8 shows the intensity imbalance before and after compensation with the tip/tilt mirror.

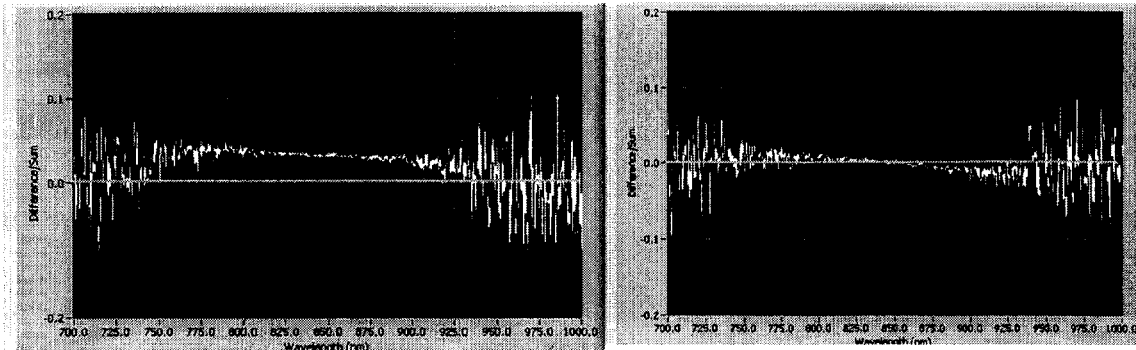


Fig. 8: Left and right show the amplitude error versus wavelength before after correction at 850nm respectively.

Measuring phase error as a function of wavelength is a bit more challenging. After trying different techniques, we found a variant of the Hilbert transform method to be a quick and accurate means of determining the phase difference between the two beams as a function of wavelength. In this approach, we first open both shutters and measure the interferogram (Fig. 9a) on the spectrometer with a known optical path length offset, introduced using the separate delay line shown in Fig. 5. The interferogram is of the form:

$$I(k) = a(k)[1 - V \cos(kX - kx_e(k))]$$

Where $k=2\pi/\lambda$ is the wave number; $a(k)$ is the source spectral envelope; V is the visibility; and $x_e(k)$ is the phase error that we want to measure. It is convenient to rewrite the above equation as:

$$I(k) = a(k) - \frac{1}{2}Va(k)\exp(kX - kx_e(k)) - \frac{1}{2}Va(k)\exp(-kX + kx_e(k))$$

We then perform a fast Fourier transform (FFT) on the interferogram (Fig. 9b) to get:

$$F\{I(k)\} = F\{a(k)\} - \frac{1}{2}V F\{a(k)\exp[kx_e(k)]\} * \delta(l + X) - \frac{1}{2}V F\{a(k)\exp[-kx_e(k)]\} * \delta(l - X)$$

If X is large, Setting the negative frequency components and the near-DC components to zero (Fig. 9c) eliminates the first two terms of the above equation. That leaves just the last term. Performing an inverse FFT of what remains yields the amplitude and phase as shown in Fig. 9d & 9e. Note that the amplitude is the source spectral envelope. The phase includes both the linear term and the phase error of interest. A polynomial fit to the phase obtained from the IFFT, provides the phase error. The coefficient of the linear term gives an accurate measure of the OPD offset and is a confirmation of that set by the delay line. The higher order terms gives the desired phase error as shown in Fig. 9f. In our experiment, we observed the phase error to be consistent with dispersion from 4 mm of BK7.

These initial tests are very promising, and at the time of this writing, the DM is being added into the proof-of-concept experiment. Therefore, we should soon be able to demonstrate phase and amplitude control over the entire 100nm bandwidth of the LED.

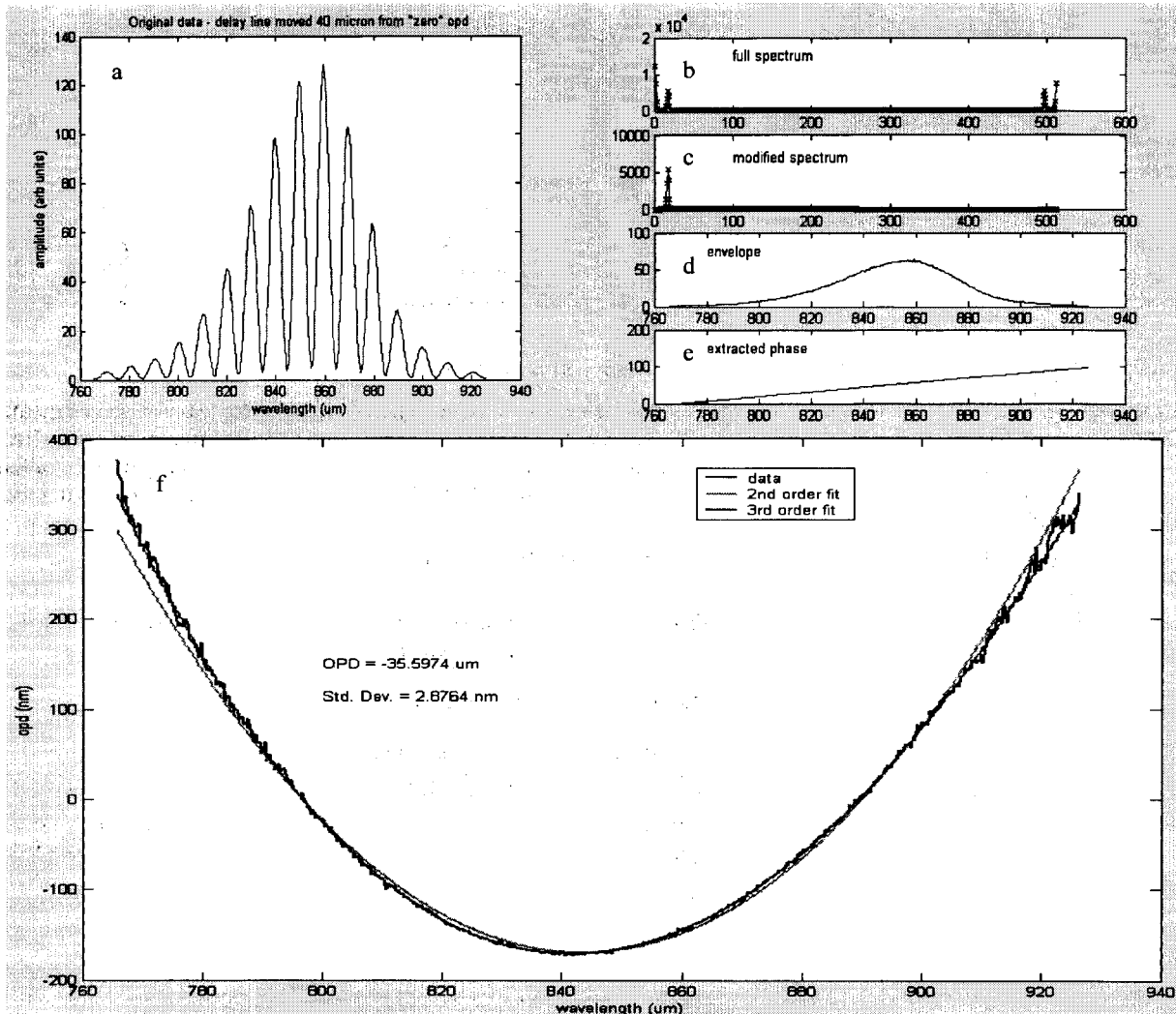


Fig. 9: Hilbert-transform based phase extraction algorithm. A) Upper left is the input spectrum as it would be detected on the spectrometer. B) Fourier transform of the spectrum. Negative frequencies extend from the right side of the plot. C) Negative frequencies have been removed. D) The extracted amplitude. E) The extracted phase. F) The higher order phase error after the bulk displacement (linear part) is removed.

4. MID-IR EXPERIMENT

For the mid-IR experiment, the optical setup will be similar to the visible/near-IR experiment (see Fig. 5) described in the previous section. Our goal is demonstrate 10^{-5} null over 8-12 um band (40% bandwidth) by end of 2006. The main differences between the mid-IR experiment and the visible experiment will be the source and detector, as well as replacing the transmissive optics such as the polarization and wavelength dispersing elements with materials suitable for the mid-IR wavelengths. Two key parts of the mid-IR experiment, the source and spectrometer, have been constructed. This section describes the work being done in parallel with the near-IR experiments to develop these key parts and identify the appropriate materials for the transmissive elements.

The setup of the part of mid-IR light source is shown in Fig. 10. The white light source is operated at a temperature of 1250-1750 K. The white light is spatially filtered and collimated with three 90° off-axis parabolic mirrors (effective focal length is 50.8 mm) and a pinhole (diameter is 75 μm). An optical chopper is placed after the pinhole. The modulation

signal of the chopper is provided to a lock-in amplifier and used as a reference signal to increase the signal-to-noise ratio of the measurements. The CO₂ laser is guided so that it is collinear with the white light for calibration of a spectrometer.

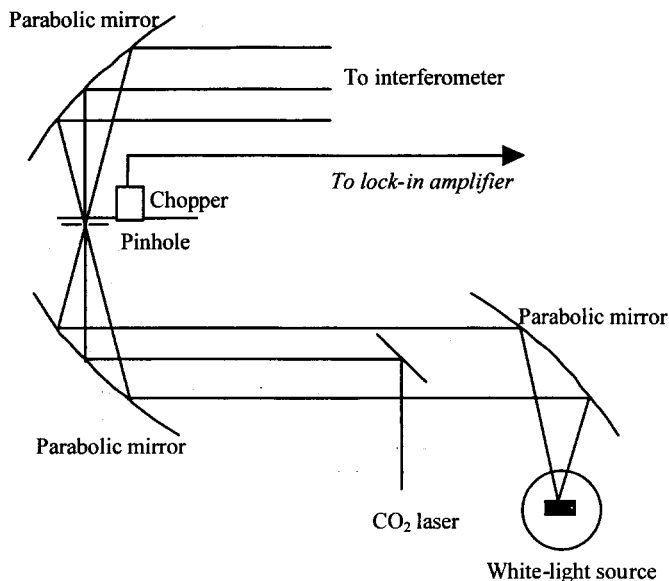


Fig. 10: Schematic layout of the mid-IR source.

While the visible/near-IR experiment uses a low-cost commercial spectrometer, similar devices in the mid-IR range are prohibitively expensive for our project. Therefore, a mid-IR spectrometer (Fig. 11) was constructed as a sensor to investigate the performance of achromatic compensation of aberration in both amplitude and phase in the future. The requirements for the wavelength range and the number of independent spectral degrees of freedom of the testbed in mid-IR are 8-12 μm and 10, respectively. The required spectral resolution for the spectrometer is set to 0.04 μm . Fig. 10 shows the schematic of the spectrometer. The combination of a grating of 60 grooves/mm and a mercury cadmium telluride (HgCdTe) detector cooled with liquid nitrogen is used as the spectrometer. The HgCdTe detector has an aperture of 0.1 mm squared, and is scanned by a computer controlled linear stage with 0.1 μm position resolution to obtain spectra. The detected signal is pre-amplified and provided to the lock-in amplifier. The spectrometer is currently being tested and calibrated. Calibration will be done with the CO₂ laser and with color filters on the white-light output.

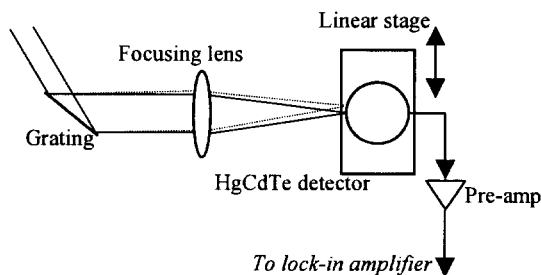


Fig 11: Schematic of the mid-IR spectrometer.

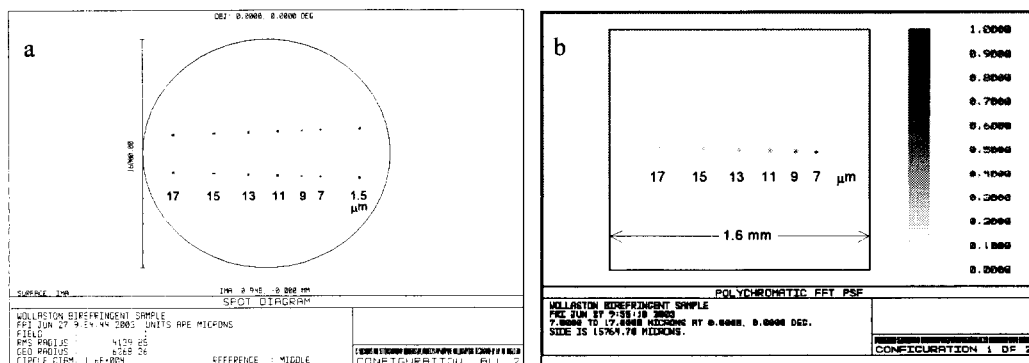


Fig. 12: Results from Zemax with a 15.3-degree KBr dispersing prism and Wollaston type CdSe prism. (a) Spot diagram at the focal plane of a 1000 mm FL paraxial lens at discrete wavelengths every 2 microns. The metrology wavelength is not dispersed too far from the mid-IR band. The polarization states are separated in the vertical direction. (b) Point spread functions for a single polarization at different mid-IR wavelengths. The reduced peak intensity is due to the larger diffraction limited spot size.

To meet our goal for this demonstration we will use an easy-to-obtain ZnSe prism with X degree wedge angle for spectral separation. For flight, KBr (Potassium Bromide) appears to be a better choice to cover the entire metrology, fringe tracking and science band (1-17 um). We will use ZnSe rather than KBr for the demonstration because ZnSe is more readily obtainable and non-hygroscopic.

We have made some progress towards obtaining polarization separation elements. Cadmium Selenide (CdSe) is the only birefringent crystal listed in the Handbook of Optics⁴ that is transparent from 1 - 17 microns. Initial modeling in Zemax⁵ indicates that CdSe will in fact sufficiently separate the polarization for the compensator to work in the mid-IR (Fig 9). We have identified a vendor, Cleveland Crystals, who can in fact make CdSe Wollaston prisms with the required specifications. The extremely slow CdSe crystal growth process, however, makes it quite expensive. We are therefore exploring polarization splitting with a wire grid on a wedge as an alternate option. We will decide on an approach by end of 2005. The optical setup of adaptive nulling interferometer in mid-IR region will be similar to that of the experiments in visible range. We are planning to do monochromatic, single polarization experiment with a tip/tilt mirror at first. And then monochromatic light source will be replaced by a white-light source and the performance of the system will be confirmed. After that, the experiment with the DM for achromatic compensation of the aberration will be demonstrated. In the same project, a single-mode fiber for mid-IR region is under development. The single-mode fiber will be used for cleaning of spatial mode of the light beam.

5. SUMMARY

We have made significant progress toward a proof-of-concept experiment at near-IR wavelengths to demonstrate that a DM system can be used to correct both the amplitude and phase of the electric field coupling into a single-mode spatial filter. The initial results from this experiment are very encouraging with amplitude and phase correction both being demonstrated at a single frequency. If successful, this compensator will ease the tight requirements on symmetry, such a compensator also enables more flexibility in the optical design and the use of much simpler, asymmetric nulling beam combiners. The next steps will be using the deformable mirror to demonstrate control over the entire spectrum in the near-IR, and eventually the mid-IR.

Additionally, a system operating at mid-infrared wavelengths is also being prepared. A source and spectrometer has been constructed, which will be integrated into the interferometer experiment in the fall of 2004.

The work described in this paper was performed at the Jet Propulsion Laboratory, California Institute of Technology, under contract with the National Aeronautics and Space Administration.

REFERENCES

1. E. Serabyn, "Nulling interferometry progress", *Proc. SPIE*, Vol. 4838, 594-608, 2003
2. C. V. M. Fridlund & P. Gondoin, The Darwin mission, *Proc. SPIE*, Vol. 4852, 394-404, 2003

3. *Terrestrial Planet Finder*, eds. Beichman, C. A., Woolf, N. J., and Lindensmith, C. A., JPL Publication 99-3, 1999
4. O. P. Lay and S. Dubovitsky, "Nulling interferometers: the importance of systematic errors and the X-Array configuration", this volume
5. Lay, O. P., Jeganathan, M., Peters, R. D., "Adaptive Nulling: A new tool for interferometric planet detection", 2003, ESA SP-539
6. Lay, O. P., Jeganathan, M., Peters, R. D., "Adaptive nulling: a new enabling technology for interferometric exo-planet detection", 2003, Proc. SPIE 5170